 doi:10.20944/preprints202105.0114.v1

Numerical simulation and experimental study on selective laser melting of 18Ni-300 maraging steel

Yan Liang [1], and Yan Biao [2,*]

[1] yanliang@sspu.edu.cn
[2] 84016@tongji.edu.cn
* Correspondence: 84016@tongji.edu.cn;

Abstract: The energy transfer process of laser selective melting is very complex. To study the effect of laser selective melting on the microstructure and properties of 18Ni-300 martensitic steel, ABAQUS was used to simulate the temperature of laser cladding 18Ni-300 martensitic steel at different time points and different laser power. The results show that the cross-section shape of the molten pool changes from round to oval with the increase of laser power.The higher the peak value of temperature time curve, the greater the temperature gradient; the laser cladding experiment of 18Ni-300 martensitic steel was carried out, and the microstructure and mechanical properties of the samples under different laser power were analyzed. The results show that with the increase of laser power, the grain size of the cladding layer becomes smaller and the microstructure becomes more coMpact; the hardness of the side surface of the sample is higher than that of the upper surface, and the tensile strength and elongation show a trend of rising first and then falling.

Keywords: selective laser melting; maraging steel, laser power; temperature field; numerical simulation

1. Introduction

Martensitic steel is the steel which has many outstanding characteristics, such as high strength, excellent toughness, good high temperature mechanical properties, small deformation during heat treatment, easy processing and no decarburization. This material is widely used in aerospace, petrochemical, mechanical mold and other industries.

With the development of 3D printing technology, SLM(selective laser melting) technology breaks through the conventional ideas of traditional manufacturing technology, has no restrictions on the complex structure of the formed parts, and can carry out small batch production, which saving production time and cost. At present, the relevant research on SLM forming martensitic steel has been mature, mainly focusing on the optimization of SLM forming process and the microstructure and properties of formed parts [1-4]. Bai Yuchao [5] used different process parameters to form 18Ni300 maraging steel by laser cladding. The results show that with the increase of laser energy density, the melting amount of metal powder increases, and the spatter of molten liquid intensifies, which leads to the formation of pores in the formed parts. Riccardo Casati et al.[6] used laser selective melting technology to form 18Ni300 maraging steel, and aged the formed parts. The results showed that after aging treatment, the microstructure changed and the amount of retained austenite, which changed with aging temperature and time. The mechanical properties of 18Ni300 maraging steel showed that the strength increased and the plasticity decreased. Tan Chaolin et al. [7] used SLM technology to manufacture high-performance 18Ni300 maraging steel, and aged the formed samples. The microstructure of SLM samples was coarse martensite. After heat treatment, the microstructure of the samples was refined, resulting in dense acicular martensite , fuzzy and irregular grain boundaries, and a large number of fine point austenite.

Martensitic steel contains more alloying elements. Solution treatment is usually carried out at about 810℃ to obtain uniform γ-austenite and prepare for the microstructure

Preprints (www.preprints.org) | NOT PEER-REVIEWED | Posted: 6 May 2021 doi:10.20944/preprints202105.0114.v1

of strengthening phase precipitated by aging [8]. After solution treatment, aging treatment (480~500℃, isothermal 3~6h) should be carried out immediately to promote the precipitation of a large number of fine and dispersed intermetallic compounds (Ni3Mo, Ni3Ti, Fe2Mo, etc.) on the martensite matrix and improve the strength of the material (strength increased by 1000 ~ 2000Mpa) [9,10]. SLM technology can reduce segregation and inhibit the development of non-equilibrium phase due to short time high speed local heat input. Therefore, M300 (SLM-M300) steel directly formed by SLM can maximize the strengthening effect of alloy elements [11,12].

In the process of laser cladding, the process parameters have a significant iMpact on the quality. In this paper, 18Ni300 martensitic steel was prepared by laser cladding technology, and the laser power was used as the parameter to explore the influence of different laser power on the microstructure and mechanical properties of the composite. ABAQUS is used to simulate the change of temperature field in the process of laser selective melting, which can provide theoretical reference for the experimental results and reduce the experimental cost.

2. Numerical simulation

2.1 Theoretical analysis and calculation

In the numerical simulation of the cladding process, the heat conduction is the main factor, only considering the convection and heat radiation between the material and air, ignoring the latent heat of phase transformation and other factors. The initial temperature of the workpiece is 20 ℃ room temperature. ABAQUS finite element analysis software is used to simulate the laser cladding process. The temperature field analysis of laser cladding is a typical nonlinear transient heat conduction problem. The nonlinear transient heat conduction equation is used, as shown in equation (1)[13]:

$$\rho c(T)\frac{\partial T}{\partial t} = \frac{\partial\left(\lambda\frac{\partial T}{\partial x}\right)}{\partial x} + \frac{\partial\left(\lambda\frac{\partial T}{\partial y}\right)}{\partial y} + \frac{\partial\left(\lambda\frac{\partial T}{\partial z}\right)}{\partial z} + Q \qquad (1)$$

Where, c is the specific heat capacity of the material; ρ is the density of the material; λ is the thermal conductivity; T is the distribution function of the temperature field; Q is the internal heat source; t is the heat transfer time. ρ. C and λ vary with temperature.The thermophysical parameters for numerical simulation are shown in Table 1.

Table 1 Thermophysical parameters of 18Ni-300

temperature	Thermal conductivity	Density	Specific heat capacity
100	22.2	7750	501
500	23.4	7750	511
1000	24.7	7750	532
1200	25.5	7750	548
1500	26.4	7750	574

In the process of laser cladding, based on the law of energy conservation, the sum of heat absorbed by the material itself, the heat of radiation loss and the heat of external convection shall be equal to the heat absorbed by the material from the laser beam. The material shall meet the heat balance equation, as shown in equation (2)[14]:

$$\lambda\frac{\partial T}{\partial n} + h(T_s - T_{ext}) + \sigma\epsilon(T_S^4 - T_O^4) = -AQ(x,y,t) \qquad (2)$$

Where :- Q (x, y, t) is the heat flux; $\frac{\partial T}{\partial n}$ is the partial derivative of the material temperature along the normal direction outside the surface; λ is the thermal conductivity; h is the convective heat transfer coefficient; T_S^4 is the surface temperature of the material; T_O^4 is the ambient temperature, σ is the Stefan Boltzmann constant, ϵ is the thermal radiation coefficient of the material surface, and a is the absorption coefficient of laser light energy on the material surface.

Preprints (www.preprints.org) | NOT PEER-REVIEWED | Posted: 6 May 2021 doi:10.20944/preprints202105.0114.v1

2.2 Numerical simulation process

In this paper, dc3d8 in ABAQUS element library is used in the numerical simulation of laser cladding. It is a linear unit with eight nodes, each representing a different temperature. According to the actual situation of the experiment, the substrate plate and scanned layeris modeled. The size of the geometric structure is shown in Figure 1

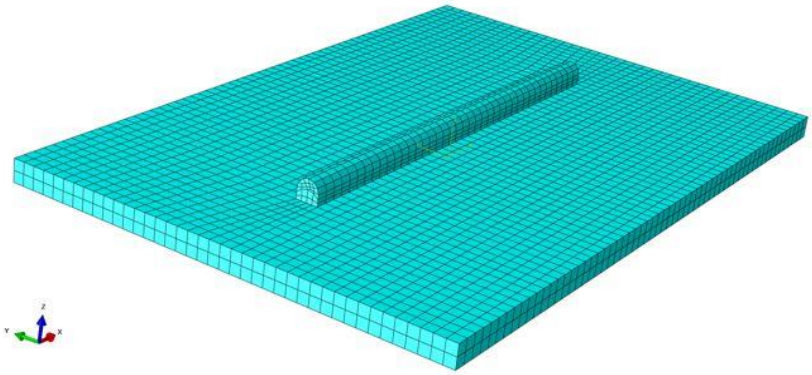

Figure 1 finite element model

To improve the calculation accuracy and shorten the calculation time, the grid size of the matrix material and cladding layer is set to 1 mm × 1 mm × 1 mm. The upper surface of 18Ni300 stainless steel powder is loaded by moving Gaussian heat source. Assuming that the heat source moves on the preset powder at a constant speed and the heat density obeys the Gaussian heat source model of normal distribution, the density expression is satisfied, as shown in equation (3) [15]:

$$q(r) = \frac{3P}{\pi R^2} exp\left(-\frac{3r^2}{R^2}\right) \qquad (3)$$

Where $q(r)$ is the heat flux at the distance r from the center of the heat source; r is the radius of the laser spot; $r = \sqrt{x^2 + y^2}$;P is the effective laser power; R is the outer diameter of the Gaussian heat source distribution.

2.3 Results and analysis

Using the above finite element model, the laser spot diameter is 70μm, the laser scanning speed is 1 000 mm/s, the laser power is 300 W, the single pass laser cladding length is 40 mm, the preset powder thickness is 2 mm, and the temperature field distribution nephogram at different times is selected, as shown in Figure 2

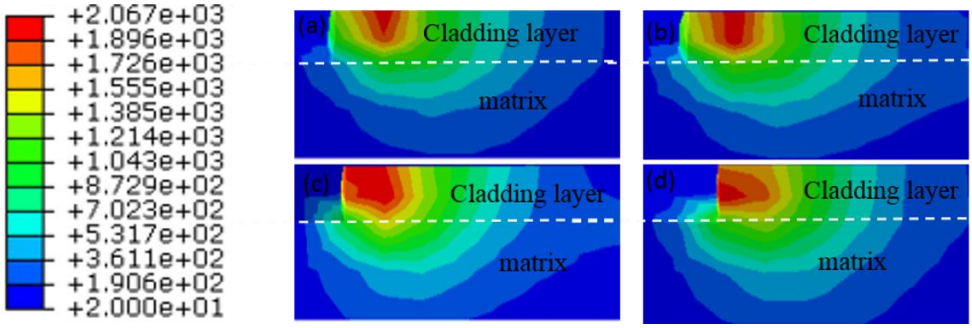

Figure. 2 evolution process of the temperature field of the weld bead at four times: (a) 0.6s, (b) 1.2s (c) 1.8s (d) 2.4s

Preprints (www.preprints.org) | NOT PEER-REVIEWED | Posted: 6 May 2021 doi:10.20944/preprints202105.0114.v1

The results show that the surface shape of the molten pool changes from round to oval and then to comet tail, which is due to the relatively low thermal conductivity of the material. In addition, the flow of the melt in the whole molten pool is mainly affected by the surface tension, while the influence of gravity and viscosity is relatively small. 1) When the laser scanning powder bed (t = 0.6s), the peak temperature in the molten pool rises rapidly to the melting temperature of the material, resulting in high temperature gradient and Marangoni convection The powder particles are affected by the energy of laser beam, so that the surface temperature of the powder particles reaches the melting point, and the melt diffuses around. However, the time of laser acting on the powder is short, and the peak value of the molten pool does not reach the boiling point of the material, so the molten pool is narrow; 2) When the contact time between the laser and the powder is enough（t = 1.2s）, and the laser energy absorbed by the powder is enough, so that the surface temperature of the molten pool almost reaches the boiling point of the material When t = 1.8s, due to the relatively low thermal conductivity of the material, the heat at the end of the molten pool can not dissipate in a short time, forming an elliptical molten pool.4) When the temperature decreases(t = 2.4s), due to evaporation and heat conduction, and the effect of recoil force decreases; Marangoni convection caused by surface tension gradient caused by temperature difference plays a major role, and the melt in the molten pool begins to move to a lower temperature position.

To further understand the temperature field changes in the process of laser cladding, the curves of temperature changes with time at different time points of single pass cladding are obtained, as shown in Figure 3. It can be seen from the temperature curve in Fig. 3 that the temperature curve at different time points presents a " mountain like Martensitic steel is the steel " change, the heating process is approximately a straight line sharp rise, and the cooling process is approximately a Mountain like, so it can be seen that the laser cladding process is a rapid heating and cooling. The main reason is that the rapid movement of the laser leads to the rapid temperature rise of the point. In the condition of natural cooling without heat source, the cooling rate gradually decreases.

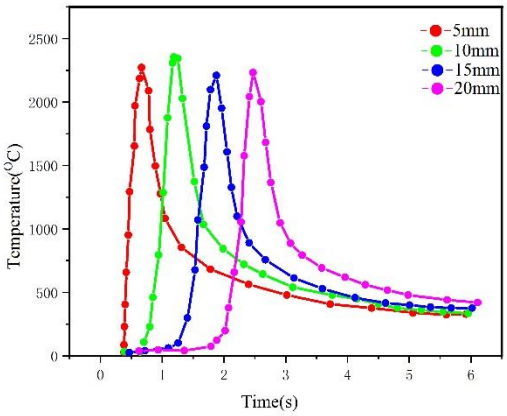

Figure 3: temperature versus time curves at different time points

To further understand the influence of different laser power on microstructure in laser cladding process, the software is used to obtain the temperature versus time curves of different laser power at 1 mm from the cladding layer surface, t = 1.2 s, as shown in Figure 4. The higher the laser power, the higher the peak temperature at the same time (t = 1.2s), and the larger the temperature gradient. The temperature gradient is the main reason for the grain size and growth trend[16].

Preprints (www.preprints.org) | NOT PEER-REVIEWED | Posted: 6 May 2021 doi:10.20944/preprints202105.0114.v1

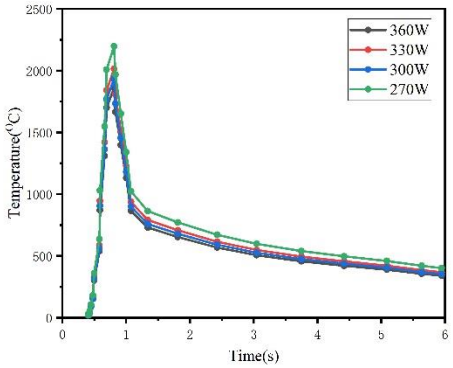

Figure. 4 temperature versus time curve of different laser power (t = 1.2s)

3 Experimental verification

3.1Experimental materials and methods

SLM-100 equipment is used to carry out relevant experiments. The maximum size of the equipment is 100 mm × 100 mm × 100 mm. SLM equipment includes single-mode CW fiber laser ylr-500-wc with maximum output power of 500 W and dynamic focusing optical scanning system hurryscan Automatic flexible powder laying system, inert gas protection system and computer forming control system can realize direct precision net forming of small and medium-sized metal components with different materials. An 18-Ni 300 maraging alloy (1.2709) supplied by Sandvik Osprey LTD (Neath, UK) asgas-atomized powder was investigated. The CoMparison of the chemical composition of declared, powder, and as-fabricated 18Ni-300 shown in Table 2.The powder morphology and particle size distribution are shown in Figure 5. The D10, D50 and D90 of 18ni300 powder were 19.0, 38.1 and 68.9 μ m, respectively. The scanning strategyadopted for the experiments is illustrated in Figure 6.

Table 2. CoMparison of the chemical composition of declared, powder, and as-fabricated 18Ni-300

Element, wt.%	Ni	Mo	Co	Ti	Cr	C	Si	Mn
Delared	17-19	4.5-5.2	8.5-10	0.6-1.2	<0.25	<0.03	<0.1	<0.15
Powder	17.8	4.5	8.6	1	0.11	<0.01	<0.032	0.002
As-Fabricated	17.7	4.6	8.5	1	0.1	<0.01	<0.033	<0.002

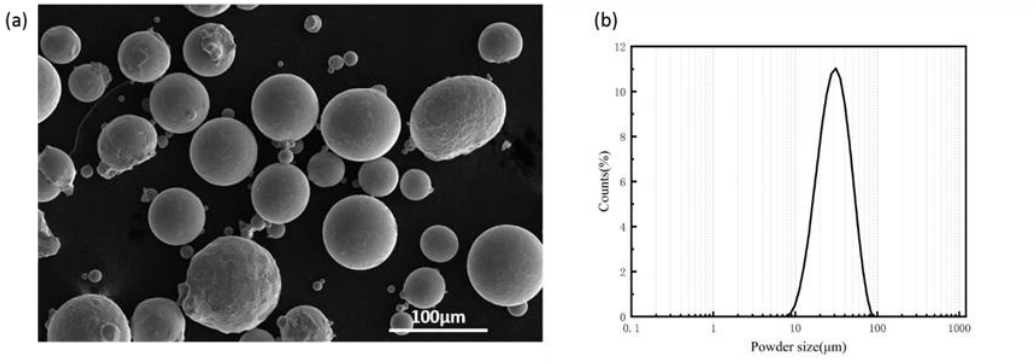

Figure. 5 SEM (a) and particle size distribution (b) of 18Ni300 powder

Preprints (www.preprints.org) | NOT PEER-REVIEWED | Posted: 6 May 2021 doi:10.20944/preprints202105.0114.v1

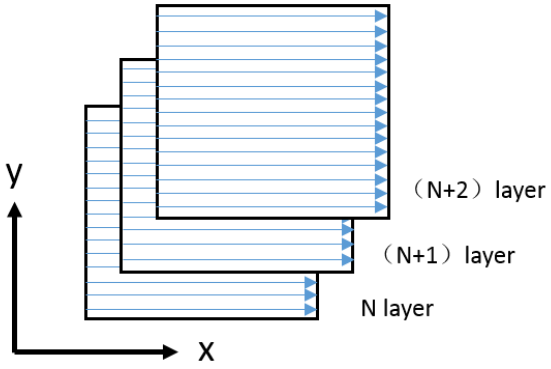

Figure. 6 illustration of the laser scanning strategy

3.2 microstructure analysis

Figure. 7 show the optical microstructure of the longitudinal section of 18Ni300 martensitic steel forming part when the scanning speed is 1000 mm/ s , the experiment adopts the scanning strategy of orthogonal layer error, the filling distance is 0.11mm and the layer thickness is 50 μm,and the laser power is 270 W, 300 W, 330 W and 360 W respectively. It can be seen that the microstructure is mainly composed of coarse martensite and a small amount of austenite. The analysis shows that in the SLM forming process, the laser beam scans the metal powder at a 90^{o} angle to form a molten pool, and the interaction between the molten pools forms a fish scale interface. When the temperature is cooled to martensite transformation temperature, part of austenite transforms into martensite rapidly. However, during solidification, solute elements are easy to produce micro-segregation at grain boundaries, which hinders martensitic transformation and causes some retained austenite to exist at grain boundaries. With the increase of laser power, the depth h and width W of weld pass increase. The reason is that with the increase of laser power, the laser energy absorbed by the powder increases in a short time, resulting in the increase of the actual lap ratio of the adjacent weld.

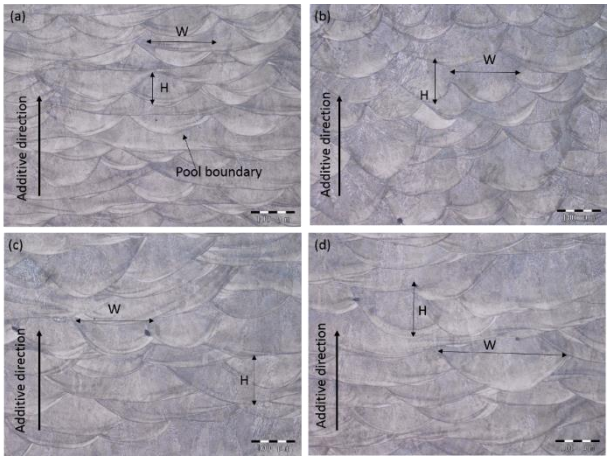

Figure.8. microstructure of longitudinal section under different laser power (a): 270W (b) 300W (c) 320W (d) 360W

To further analyze and coMpare the internal structure of the printed samples under different laser power, the internal microstructure was observed under high-power SEM, as shown in Figure 8. There are obvious grain boundaries in the molten pool, and the microstructure in the central region is mainly cellular crystal. The formation of this kind of crystal is mainly related to the cooling rate. The faster the cooling rate is, the more can promote the transformation of the initially generated planar crystal to cellular crystal, and the cell crystal spacing becomes smaller with the increase of laser power. In the process of SLM printing, the powder is heated and melted into molten metal. When the molten metal is continuously deposited to the crystal nucleus, the grains grow continuously, thus realizing the solidification of the molten metal[17]. According to the solidification theory, the grain can be refined by reducing the growth rate and increasing the nucleation rate, and

Preprints (www.preprints.org) | NOT PEER-REVIEWED | Posted: 6 May 2021 doi:10.20944/preprints202105.0114.v1

the scanning electron microscope can be used to analyze the microstructure When the laser speed is fixed, the higher the laser power is, the higher the energy power density is, which leads to higher heat input and higher bath temperature. A large amount of energy is gathered around the grains to provide sufficient energy for the growth of the grains. The cooling and solidification speed becomes slower, which slows down the nucleation rate of the inner cellular crystals and forms larger cellular crystals. With the increase of laser power, the power density gradually increases, the cooling time becomes longer, the cooling and solidification speed is accelerated, and the crystal cell is gradually refined.

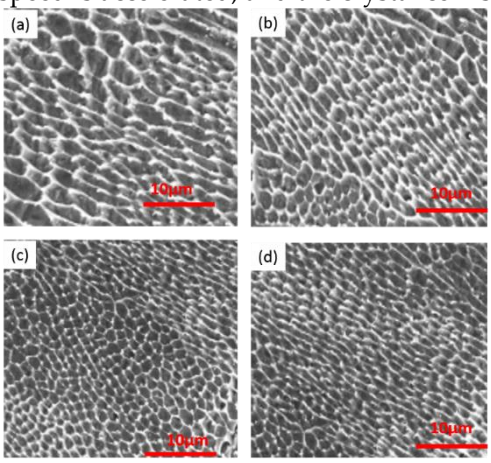

Figure 8. SEM morphology of longitudinal section of printed sample under different laser power (a): 270W (b) 300W (c) 320W (d) 360W

3.3 mechanical property analysis

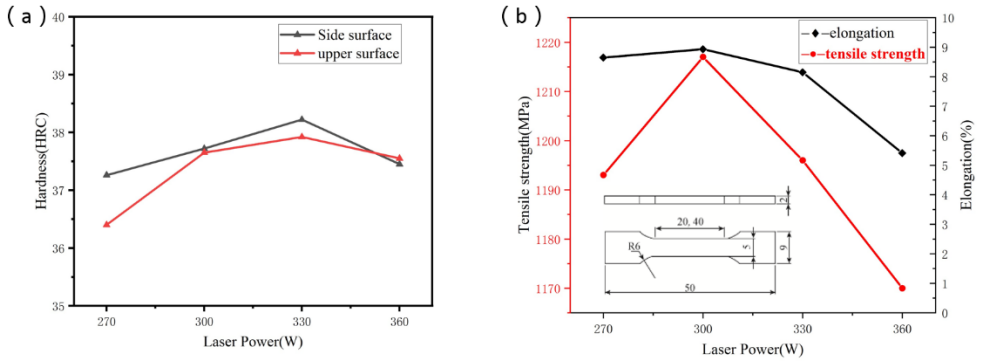

Figure 9. Effect of laser power on mechanical properties. (a) Surface hardness; (b) tensile properties

The tensile test was carried out on CMT 5105 electronic universal testing machine, and the hardness was measured by DHV-1000Z digital micro Vickers hardness tester. Figure 8 shows the hardness figure 9 (a) and tensile property figure 9 (b) of the sample under corresponding parameters. It can be seen from Fig. 9 (a) that the law of the hardness of the side surface of the sample is the same as that of the upper surface. The hardness of the side surface of the printed sample is higher than that of the upper surface under the same laser power. This is because in the process of layer by layer stacking, the martensite structure formed will extend along the forming direction to the epitaxial boundary of the weld channel, which makes the side surface higher than the upper surface. It can be seen from Fig. 9 (b) that the tensile strength and elongation of the sample increase first and then decrease. When the laser power is 270W, the tensile strength is 1192Mpa, the upper surface microhardness is HRC36.3, the side surface microhardness is HRC37.2, and the elongation after fracture is 8.55%; when the laser power is 300W, the tensile strength is 1217Mpa, the upper surface microhardness is HRC37.5, and the side surface microhardness is HRC37.6 The laser power was 330W, the tensile strength was 1195Mpa, the microhardness of upper surface was HRC37.7, the microhardness of side surface was HRC38.2,

Preprints (www.preprints.org) | NOT PEER-REVIEWED | Posted: 6 May 2021 doi:10.20944/preprints202105.0114.v1

and the elongation after fracture was 8.1% When the laser power is 360W, the tensile strength is 1171Mpa, the upper surface microhardness is HRC37.4, the side surface microhardness is HRC37.2, and the elongation after fracture is 5.5%; when the laser power is 300W, the comprehensive mechanical properties of the sample are the best.

To further study the fracture mechanism of tensile fracture, SEM is used to observe the fracture surface of tensile specimen. From Figure *10*, it can be seen that the fracture surface of tensile specimens is composed of dimples of different sizes. The main reason for the above brittle plastic transformation mechanism is the influence of energy density. The excessive energy density makes the temperature of the forming process rise sharply, and the internal residual stress of the sample is large, which increases the internal brittleness, which leads to premature failure of the forming sample. When the laser power is 270 W, although the internal grain size is gradually refined and the grain boundary increases, which hinders the crack propagation to a certain extent; however, due to the low power density, more defects appear in the forming process, and not only deep holes appear on the tensile fracture surface, but also large granular inclusions appear in the holes. As shown in Figure*10* (a); When the laser power is 300W, a large number of equiaxed dimples are distributed on the fracture surface. These dimples are not only evenly distributed, but also have large depth, showing good plasticity, as shown in Figure *10* (b). Therefore, the tensile strength and elongation of the sample are the highest; When the laser power is 330W, the dimple size of the fracture surface increases gradually, and the depth increases. The fracture surface also has obvious tear marks, which reduces the tensile properties of the sample as shown in Figure *10* (c). When th*e laser power increases to 360W.A*s shown in Figure *10* (*d*), the fracture mode changes to plastic fracture, the number of dimples on the surface increases, and there are granular inclusions on the fracture surface.

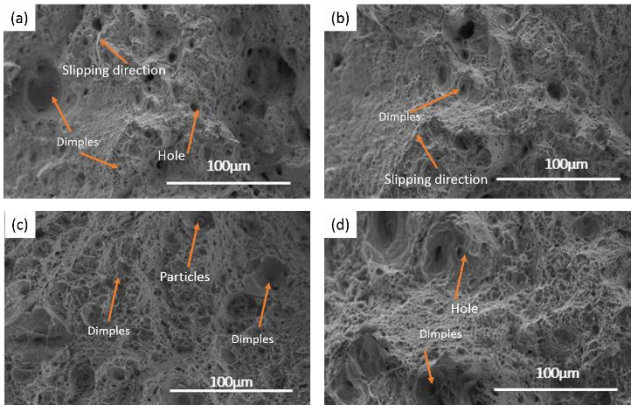

Figure 10. tensile fracture morphology of printed samples under different laser power (a): 270W (b) 300W (c) 320W (d) 360W

4. Conclusions

In this study, we numerically simulate the temperature field, molten pool and temperature time curve at different time points and different laser power. The effects of different laser power on the microstructure, grain size and mechanical properties of SLM 18Ni-300 martensitic steel were analyzed. The main conclusions are as follows：

- When the laser just scans the powder bed (t = 0.6s), the shape of the molten pool is quasi circular. When the laser time fully contacts with the powder bed (t = 1.2s), the shape of the molten pool is elliptical. When the laser time fully contacts with the powder bed (t = 2.4S), the shape of the molten pool is elliptical and comet like;

- The thermal cycle curve of different laser power is simulated by numerical simulation. The thermal cycle curve at this point is zigzag, and the maximum temperature increases with the increase of laser power. The microstructure shows that with the increase of laser power, the grains of the cladding layer become smaller, the grains are fine equiaxed grains, and the microstructure is more coMpact.

- The results show that the variation rule of the side surface hardness of the sample under different laser power is the same as that of the upper surface, and the side surface hardness of the sample printed under the same laser power is higher than that of the upper surface; the tensile strength curve shows a "low high low" distribution trend, and the comprehensive mechanical properties of the sample are the best when the laser power is 300 W and the scanning speed is 1000 mm/s . The tensile strength, microhardness and elongation after fracture are 1217Mpa, HRC 37.5 and 37.6 ,8.44% respectively.

References

1. Yao, Y.; Wang, K.; Wang, X.; Li, L.; Yan, F. Microstructural Heterogeneity and Mechanical Anisotropy of 18Ni-330 Maraging Steel Fabricated by Selective Laser Melting: The Effect of Build Orientation and Height. J. Mater. Res. **2020**, 35 (15), 2065-2076.
2. Oliveira, A.R.; Diaz, J.; Nizes, A.; Jardini, A.L.; Julián, V. Investigation of Building Orientation and Aging on Strength–Stiffness Performance of Additively Manufactured Maraging Steel. J. Mater. Eng. Perform. **2021**, 30 (2).
3. Lai, L.; Zhen-Lin, X.U.; Yi-Zhu, H.E. Effect of Heat Treatment on Microstructure and Corrosion Properties of SLM 18Ni300 Maraging Steel. Surface Technology **2019**.
4. Kucerova, L.; Zetkova, I.; Jandova, A.; Bystriansk, M. Microstructural Characterisation and In-Situ Straining of Additive-Manufactured X3NiCoMoTi 18-9-5 Maraging Steel. Materials Science and Engineering A **2019**, 750 (MAR.18), 70-80.
5. Bai, Y.; Yang, Y.; Wang, D.; Zhang, M. Influence Mechanism of Parameters Process and Mechanical Properties Evolution Mechanism of Maraging Steel 300 by Selective Laser Melting. Materials Science and Engineering: A **2017**.
6. Riccardo, C.; Jannis, L.; Ausonio, T.; Maurizio, V. Aging Behaviour and Mechanical Performance of 18-Ni 300 Steel Processed by Selective Laser Melting. Metals - Open Access Metallurgy Journal **2016**, 6 (9), 218.
7. Cta, B.; Kza, B.; Wm, B.; Pz, B.; Min, L.B.; Tk, A. Microstructural Evolution, Nanoprecipitation Behavior and Mechanical Properties of Selective Laser Melted High-Performance Grade 300 Maraging Steel - ScienceDirect. Materials & Design **2017**, 134, 23-34.
8. Yang ZY; G Qi; D Yali.; Investigation on the Technology for Improving Toughness of Maraging Steel by Lowering Solution Treatment Temperature. new technology and new process, **2018**, 000 (005), 1-3.
9. Yin, Z.; Hiaodong, L.I.; Haibin, L.I.; Lai, Z. Aging Mechanism of 18Ni Maraging steel.Acta Metallrugics Sinica **1995**.
10. Z Weigang. Microstructure and properties of 2800Mpa maraging steel. Kunming University of science and technology, **2017**
11. Jie, Z.; Shuai, L.; Wei, Q.; Shi, Y.; Wang, L.; Guo, L. Cracking Behavior and Inhibiting Process of Inconel 625 Alloy Formed by Selective Laser Melting. Chinese Journal of Rare Metals **2015**.
12. Kempen, K.; Yasa, E.; Thijs, L.; Kruth, J.P.; Humbeeck, J.V. Microstructure and Mechanical Properties of Selective Laser Melted 18Ni-300 Steel. Physics Procedia **2011**, 12, 255-263.
13. Sohail, M.; Han, S.W.; Na, S.J.; Gumenyuk, A.; Rethmeier, M. Characteristics of Weld Pool Behavior in Laser Welding with Various Power Inputs. Weld. World **2014**, 58 (3), 269-277.
14. Parekh, R.; Buddu, R.K.; Patel, R.I. Multiphysics Simulation of Laser Cladding Process to Study the Effect of Process Parameters on Clad Geometry. Procedia Technology **2016**, 23, 529-536.
15. Simulation Study On Laser Cladding On Preplaced Powder Layer with a Tailored Laser Heat Source. Optics & Laser Technology **2013**.
16. L Gang. Simulation of grain growth in HAZ by diffusion interface field variable model. Zhengzhou University, **2006**
17. G Yimin, principle of metal solidification: **2010**